First-principles calculations of electron-energy-loss near-edge structure and near-edge x-ray-absorption fine structure of BN polytypes using model clusters

Isao Tanaka and Hiroyuki Araki
Department of Energy Science and Technology, Kyoto University, Sakyo, Kyoto 606-8501, Japan

Masato Yoshiya, Teruyasu Mizoguchi, Kazuyoshi Ogasawara, and Hirohiko Adachi
Department of Materials Science and Engineering, Kyoto University, Sakyo, Kyoto 606-8501, Japan
(Received 28 December 1998)

Effects of a core hole in the unoccupied density of states are systematically studied using model clusters of *h*-BN, *c*-BN, and *w*-BN, in order to reproduce and interpret experimental electron-energy-loss near-edge structure /near-edge x-ray absorption fine structure at both B- and N-K edges. Wave functions are found to localize significantly near the core hole, thereby changing their energies as well as spatial distribution. They are very different from the Bloch states assumed in a band-structure calculation on the basis of a structural unit cell. When the presence of the core hole is ignored, in other words at the ground state, small clusters such as *h*-(B_7N_{12}) exhibit better agreement with the experiment as compared with large clusters such as *h*-($B_{91}N_{108}$) because wave functions are made to localize in the small clusters. Features appeared in the experimental spectra are interpreted in terms of chemical bondings among atomic orbitals using overlap population diagrams. Absolute transition energies by Slater's transition state method agree with experimental values within an error of 1%. [S0163-1829(99)12131-3]

I. INTRODUCTION

A high spatial-resolution analytical electron microscope equipped by electron energy-loss spectroscopy (EELS) is challenging to obtain spectra with single atomic column resolution.[1] Since the near-edge structure of EELS (ELNES) conveys information on chemical bonding from the illuminated area, one can expect to identify a local chemical environment of atomic-sized substances, such as interfaces, nanoprecipitates, and large molecules, directly by experiments. When ELNES is taken by transmission electron microscopy, it is analogous to near-edge x-ray absorption fine structures (NEXAFS) that is also widely utilized in physics/chemistry of condensed matter.

Recently, ELNES technique has been successfully applied to investigate C_{60} (fullerens),[2] higher fullerens,[2] carbon nanotubes,[3] and BN nanotubes.[4,5] Carbon-K-edge spectrum from C_{60} is found to be sensibly different from that of graphite reflecting the difference in the manner of C-C bondings. The C-K edge spectrum from C nanotubes looks similar to graphite. Stephan *et al.*[3] pointed out that a subtle difference in the spectra between nanotubes and graphite can be ascribed to the curvature of graphitelike layers in nanotubes. Similar results have been reported for BN nanotubes.[5]

Despite advances in experimental technique of ELNES, a theoretical method to analyze the spectra is still immature. B-K-edge ELNES from hexagonal BN (*h*-BN) resembles C-K-edge ELNES from graphite whose first two intense peaks have been ascribed to π^* and σ^* orbitals since literatures in the 1940s.[6,7] However, assignment of higher-energy peaks has not been well established to date. It is true that a number of band-structure calculations of graphite have thus far been made,[3,8–12] since it is a good reference material having a layered structure. However, results from early theoretical studies by semiempirical methods are different from modern theoretical results, especially at higher energies. Although spectral features in early experimental data measured with relatively low-energy resolution were somehow reproduced[11–14] by the early theoretical methods, they should be reexamined.

Most of the theoretical calculations that have been used to compare with the experimental spectra were done for the ground state. In other words, the presence of a core hole has been completely neglected. On the absorption phenomenon, an electron is excited from a core level to an unoccupied orbital leaving a core hole. Unoccupied band structure is, in general, changed by the presence of the core hole. Calculation at the ground state reproduces the experimental spectrum only when the core-hole effect is not significant.

The influence of the core hole has been estimated mainly by increasing the atomic number of the nucleus undergoing excitation by one, which is called $Z+1$ approximation,[15] or final-state approximation. Since many of the modern first-principles calculations freeze core states for computational economy, the $Z+1$ approximation is a convenient way to include the effect. However, the validity of the approximation should be carefully examined. In addition, since wave functions are localized near the core-excited atom, a sufficiently large super-cell size should be chosen when one uses the band-structure method. Regarding graphite, Mele and Ritsko[16] find that the effect of the core hole on the unoccupied density of states is significant by an empirical method. Ahuja *et al.*[17] recently performed more reliable calculations using a full-potential linearized muffin-tin orbital method for a super cell composed of 50 atoms. They also reported experimental NEXAFS with a high-energy resolution of 0.13 eV, and compared the spectra with theoretical ones. According to them, both the σ^* and π^* excitons are localized in the

vicinity of the core-excited atom. They concluded that the inclusion of the core hole was essential. Unfortunately, they did not refer to the origin of the high-energy peaks.

We have recently demonstrated that inclusion of a core hole in an all-electron calculation notably improves the theoretical ELNES/NEXAFS especially for α-Al_2O_3 at the Al-L_{23} edge using a first-principles molecular-orbital (MO) method.[18] An unoccupied orbital was found to localize significantly when an Al-2p hole was included, which changed remarkably the shape of the ELNES/NEXAFS near the onset of the spectrum. In addition, an absolute transition energy was reproduced within an error of a few percent by the calculation for the Slater's transition state[19] in which half of the electron in a core orbital is removed to put into the lowest unoccupied orbital. Calculation of the localized states by a band-structure method requires a large supercell in general, which is very time consuming. Cluster calculations with varying cluster size is, therefore, a practically useful approach for the reproduction of ELNES/NEXAFS.

In the present study, we perform first-principles MO calculations of BN polytypes using model clusters. Results of first-principle band-structure calculations at the ground state for BN polytypes can be found in (Ref. 20) and also references cited therein. However, all of these calculations were conducted for the ground state. No first-principles calculation for a core-holed configuration has thus far been reported. Moscovici *et al.*[21] recently reported the B- and N-K-edge NEXAFS from h-BN with high energy resolution of 0.2 to 0.4 eV. Theoretical calculations can, therefore, be put to the good test. The present paper aims at not only the reproduction of the experimental spectra, but also interpretation of the origin of spectral features from the viewpoint of interactions among atomic orbitals.

II. COMPUTATIONAL PROCEDURES

First-principles MO calculations were performed using a program SCAT[22] based on the discrete variational $X\alpha$ (DV-$X\alpha$) method.[23] Numerical atomic orbitals were used as basis functions. They were generated flexibly to a given chemical environment by solving radial part Schrödinger equations. All integrations were made in a numerical manner. Calculations were done for model clusters that were cut from real crystals. In the case of h-BN, two kinds of clusters composed of a single graphite layer and three layers were first compared: Their results were found to be identical regarding the spectral shape. Then, the size of the single-layered cluster was changed from 19 to 199 atoms in order to see the size dependence. Clusters were embedded in Madelung potential generated by point charges located at the external atomic sites. Minimal basis sets were used in order to clarify the simple relationship between spectral features and chemical bondings except for the case otherwise noted. They are 1s, 2s, and 2p for both B and N.

Self-consistent calculations were made for three electronic configurations, namely, ground state (initial state), final state with the presence of a core hole, and the Slater's transition state[19] in which a half electron was removed from a core orbital to fill the lowest unoccupied orbital. Effect of the presence of a core hole can be evaluated in this way. Moreover, the absolute transition energy, that is, the total energy difference between the initial and the final states, can be well approximated by the difference of one-electron orbital energies obtained for the Slater's transition state[19] when temporary spin polarization associated with the transition is allowed.

The overlap population between ith atomic orbital and jth atomic orbital at the lth MO is given by

$$Q_{ij}^{l}=C_{il}C_{jl}S_{ij}, \tag{1}$$

where S_{ij} is the overlap integral given by

$$\int \chi_i^*(\mathbf{r})\chi_j(\mathbf{r})d\mathbf{r}=S_{ij}. \tag{2}$$

χ_i and C_{il} are ith atomic orbital and its coefficient for the lth MO.

The photoabsorption cross section (PACS) is proportional to the oscillator strength for the transition for photon absorption between ith core state and lth MO, which is given by

$$I_{i\rightarrow l}\propto \Delta E|\langle l|\mathbf{r}|i\rangle|, \tag{3}$$

where ΔE represents the transition energy. In the present paper, the value was obtained directly by the numerical integration of the dipole matrix when necessary. Density of states (DOS) and PACS were obtained by convolution of discrete values at each lth MO by Gaussian functions of 1.0-eV full width at half maximum (FWHM). Overlap population diagrams were made in the same way using values given by Eq. (1).

III. HEXAGONAL BORON NITRIDE (h-BN)

Experimental spectrum of h-BN at the B-K edge[21,24] (Fig. 1) resembles that of graphite at the C-K edge, since the major component of the conduction band is B-2sp orbitals. It is true that some experimental paper reported that the first peak located at 191 eV (that will be hereafter called peak A) did not vanish even when the spectrum was taken with a $q\perp c$ condition, where q is the momentum-transfer vector and c is the unit vector toward c axis. However, recent NEXAFS of a single crystal highly oriented pyrolitic boron nitride by Moscovici *et al.*[21] and x-ray Raman-scattering spectra of a single crystal BN by Watanabe *et al.*[25] found that peak A entirely vanishes under the $q\perp c$ condition. It confirms that the origin of peak A is the wave function perpendicular to the graphite layer, which is consistent with the assignment of peak A to be π^*. The second intense peak located at 198 eV (peak B) has been ascribed to σ^* interaction. The x-ray Raman-scattering spectra found that peak B did not vanish under the $q\parallel c$ condition, although it is much weaker than that measured under the $q\perp c$ condition. It means that the origin of peak B is not purely of p_{xy} type. A small peak can be found between peaks A and B only when the energy resolution is high[5,21] in both NEXAFS and ELNES. Three more features can be at least seen above peak B. Peaks C and D can be clearly separated only when the energy resolution is high.[21] Peak E is broad even when measured with high resolution, and it is more clearly seen under the $q\perp c$ condition.

Figure 1 also displays B-2p partial density of states (PDOS) obtained locally at the center of three types of clusters. Calculations are done for ground (initial) states, Slater's

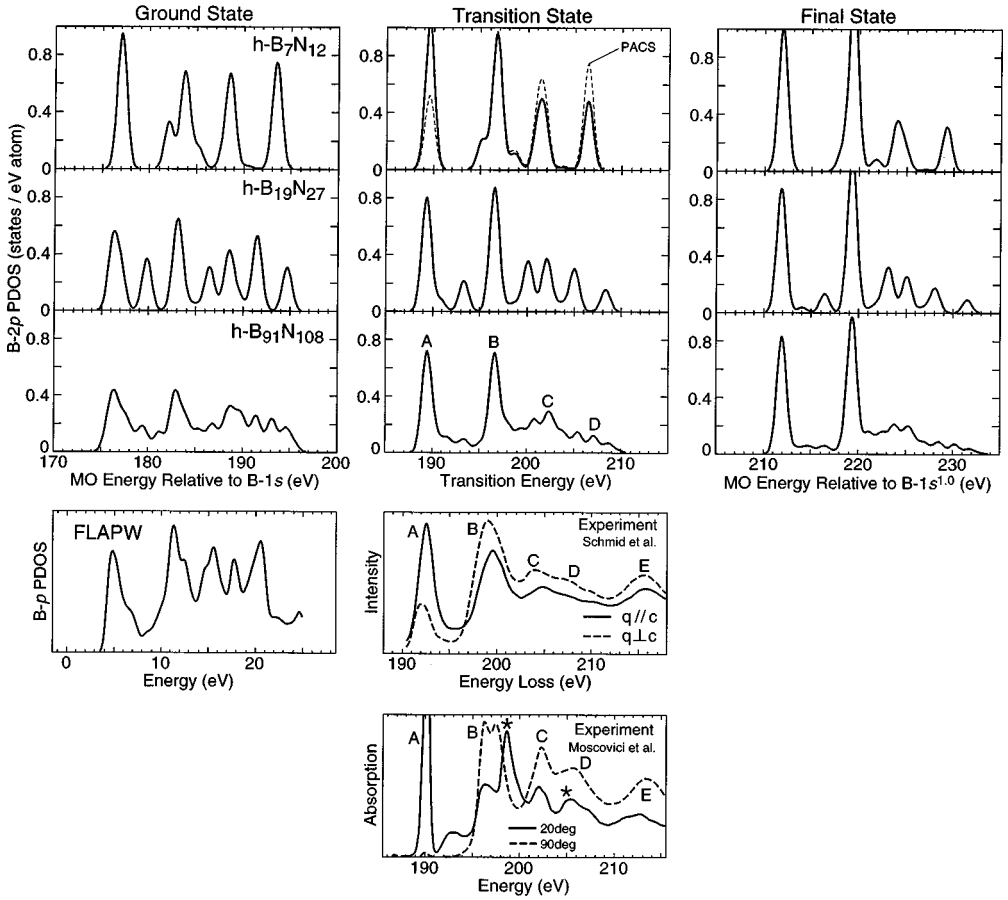

FIG. 1. Local B-2p PDOS for (left column) ground states, (middle column) Slater's transition states, and (right column) final states at the center of model clusters of h-BN. Spin polarization is allowed only for the transition-state calculations. Clusters are (1st row) h-$(B_7N_{12})^{15-}$, (2nd row) h-$(B_{19}N_{27})^{24-}$, and (3rd row) h-$(B_{91}N_{108})^{51-}$. The FLAPW result at the ground state, and experimental B-K-edge ELNES by Schmid (Ref. 24) and NEXAFS by Moscovici *et al.* (Ref. 21) are compared. The NEXAFS was measured at two polarization angles (20 and 90 deg.). The peaks denoted by an asterisk were ascribed to the ghost of the nitrogen-edge spectrum due to the presence of a second harmonic in the monochromatic beam.

transition states, and final states. PACS are also calculated as shown by broken curves. PACS is found to be well approximated by the corresponding PDOS except for a small difference in intensities. We have reported the agreement between PACS and PDOS in a number of systems using the present computational method (see, for example, Ref. 18). This can be ascribed to the use of ''optimized'' numerical atomic orbitals.

At the ground state, local PDOS at the center of the cluster is notably dependent on the cluster size. The dependence may be ascribed to the mixture of surface states at the center of the cluster. As for peaks A and B, the ground state using the largest cluster, $(B_9N_{108})^{51-}$, agrees with the B-p partial density of states by the full potential linearized augmented plane wave (FLAPW) band-structure calculation.[26] DOS of the FLAPW by the tetrahedron method is broadened by convoluting Gaussian function of 0.5-eV FWHM. They also well reproduce the DOS in literature[20] around peaks A and B. Disagreements in higher-energy features may be due to the use of the minimal basis set as will be seen with Fig. 8.

When a half-filled core hole is present, relative intensities of peaks A and B compared with other peaks become much stronger. As a result, cluster-size dependence of the PDOS is seemingly less significant when the core hole is present. The wave functions responsible for both peaks A and B are significantly localized due to the presence of the core hole. A contour map of the wave function responsible for peak A is shown in Fig. 2. The contour map at 26 pm above the graphitic plane is shown. In the smallest cluster, $(B_7N_{12})^{15-}$, the wave function is mainly composed of $2p_z$ orbital of a central B atom. It shows π^* type antibonding interaction with its neighboring N atoms. With the increase of cluster size, the wave function at the ground state becomes delocalized as in the case of the largest cluster $(B_{91}N_{108})^{51-}$. Band-structure calculation for h-BN shows that peak A at the ground state is originated from K and M points in the first Brillouin zone.[20] The wave function of the cluster $(B_{91}N_{108})^{51-}$ at the ground state shown in Fig. 2 corresponds to that of the K point in the band-structure calculation. When a core hole is present, the wave function is significantly localized. It is clearly seen in the largest cluster, $(B_{91}N_{108})^{51-}$. However, in the smallest cluster, the magnitude of localization is almost invisible in the contour map. The wave function is already localized even at the ground state when the smallest cluster is used. B-2p PDOS is not changed significantly by the presence of the core hole either, as can be seen in Fig. 1 for the $(B_7N_{12})^{15-}$ cluster. Rough agreement

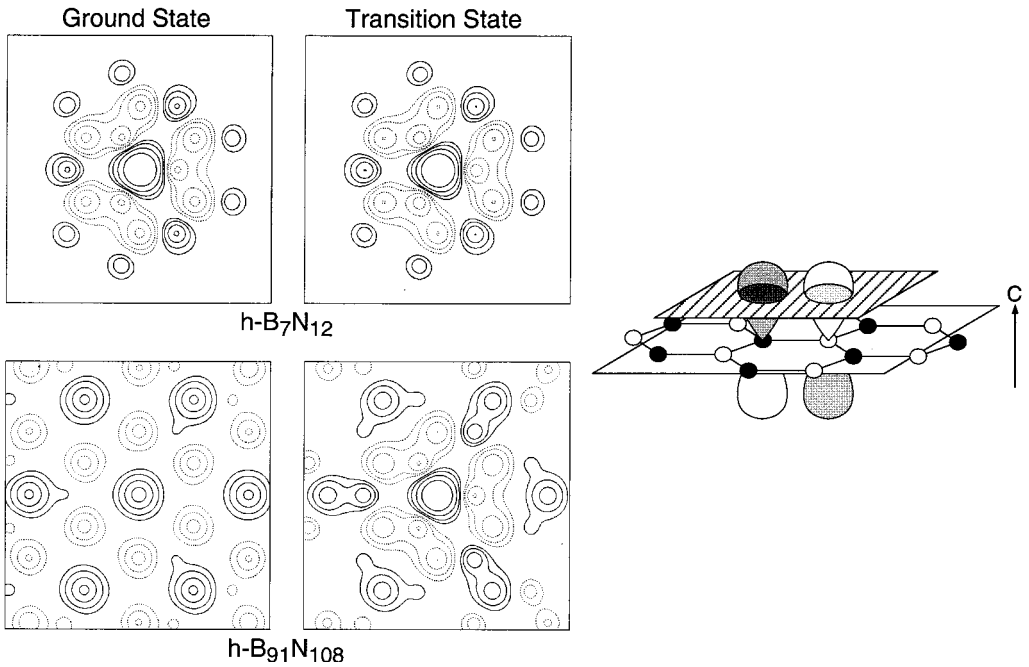

FIG. 2. Contour map of wave functions responsible for peak A shown in Fig. 1 obtained for the $(B_7N_{12})^{15-}$ cluster. Curves are drawn for ± 0.01, ± 0.02, ± 0.04, and ± 0.08, respectively. Solid and dotted curves are for positive values and negative values, respectively.

with the experimental spectra and the B-2p PDOS of the small cluster at the ground state is not accidental. Use of the small cluster forces to localize the wave function similar to the case when a core hole is present.

In order to understand the origin of peaks from the viewpoint of chemical bonding in a simple manner, overlap population diagram regarding B-2p_z orbital for the smallest cluster are plotted as shown in Fig. 3. An extra peak denoted by A′ can be seen at around 195 eV, which corresponds to the low-energy shoulder of peak B. The wave functions responsible for peaks A and A′ are both antibonding with respect to the nearest-neighbor B-2p_z-N-2p_z interaction around the central B atom. However, the manner of second-neighbor B-2p_z-B-2p_z interaction is opposite in sign between peaks A and A′, although the magnitude of the overlap population for B-B is an order of magnitude smaller than that of the B-N. These wave functions are drawn in Fig. 4. Contribution of the 2p_z orbitals cannot be found above peak A′. Peak A′ is originated from the wave function that contains a maximum number of nodes, thus having the highest energy within

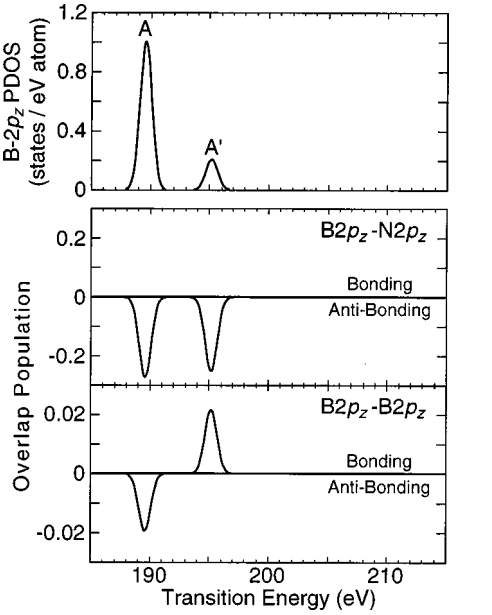

FIG. 3. Local B2p_z DOS and overlap population diagrams for the B2p_z-N2p_z and B2p_z-B2p_z interactions obtained for Slater's transition state of the $(B_7N_{12})^{15-}$ cluster.

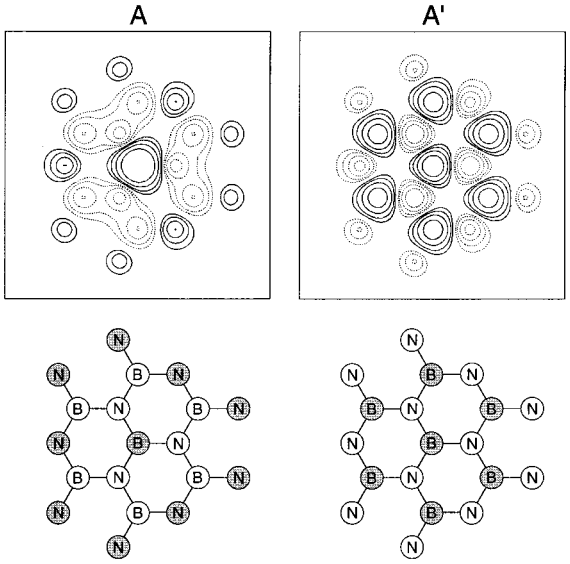

FIG. 4. Contour maps of wave functions responsible for peak A and A′ shown in Fig. 3 obtained for the $(B_7N_{12})^{15-}$ cluster at the transition state. Curves are drawn for ± 0.01, ± 0.02, ± 0.04, and ± 0.08, respectively. Solid and dotted curves are for positive values and negative values, respectively.

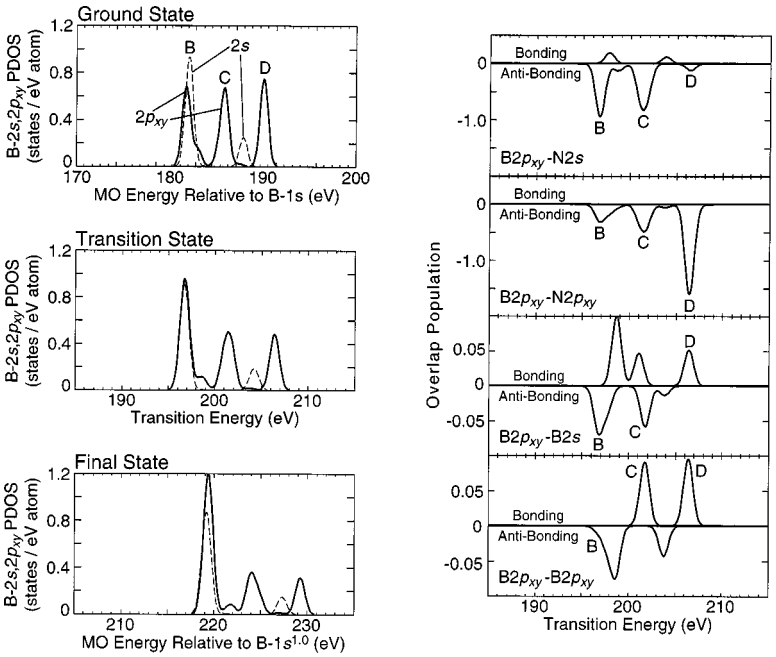

FIG. 5. (Left) Local B2s and p_{xy} PDOS for three states by the $(B_7N_{12})^{15-}$ cluster. (Right) Overlap population diagrams obtained for the calculation for the transition state.

molecular orbitals made by the B-2p_z orbitals. No contribution of B-2s or B-2p_{xy} orbitals can be seen for peaks A and A′.

Although the B-K edge spectrum corresponds to the B-p PDOS because of the electric dipole selection rule, B-2s orbital plays an important role in determining spectral shape. Peak B is usually denoted simply by the σ^* peak. However, PDOS shown in Fig. 5 clearly indicates that the B-2s orbital significantly hybridizes with the B-2p_{xy} orbitals in the energy region around peak B at the ground state. When a core hole is included, localization of the B-2p_{xy} orbitals is more significant than that of the B-2s orbital. As can be seen in the overlap population diagrams shown in Fig. 5, the nearest-neighbor interaction between B-2p_{xy} and N-2s, 2p_{xy} for peaks B, C, and D are all antibonding around the central B atom. The antibonding between N-2s and B-2p_{xy} is significant for peaks B and C. On the other hand, N-2p_{xy}-B-2p_{xy} antibonding is significant for peak D. Both B-2s and N-2s components thus contribute significantly to peak B. In addition to the contribution of the 2s components, the wave functions responsible for peaks B, C, and D can be discriminated by the number of the nodes, which can be seen by the overlap population diagrams of the 2nd neighbor B-B interactions. The situation is similar to the A-A′ splitting, but this is more complicated because of the mixture of 2s and 2p_{xy} orbitals. Molecular orbitals having a B-2p_{xy} component at the center of the cluster under the C_{3v} symmetry can be categorized in a point group of e symmetry that are doubly degenerated. Contour maps of pairs of the doubly degenerated wave functions responsible for peaks B, C, and D in the smallest cluster are shown in Fig. 6. As can be clearly seen, the number of nodes increases in the order of peaks B, C, and D. Assignment of peaks can be made in the same way using the largest cluster when a half-filled core hole is included as shown in Fig. 7. Peaks B, C, and D are different in both the contribution of the 2s components and the number of nodes in the molecular orbitals.

Peak E located at around 215 eV is not reproduced by the above calculations even when a core hole is included. We use minimal basis sets in the above calculations in order to understand the orbital interactions most clearly. However, highest eigenvalues of molecular orbitals in the above calculations are approximately 20 eV measured from peak A. It means peaks at higher energies are not able to be reproduced.

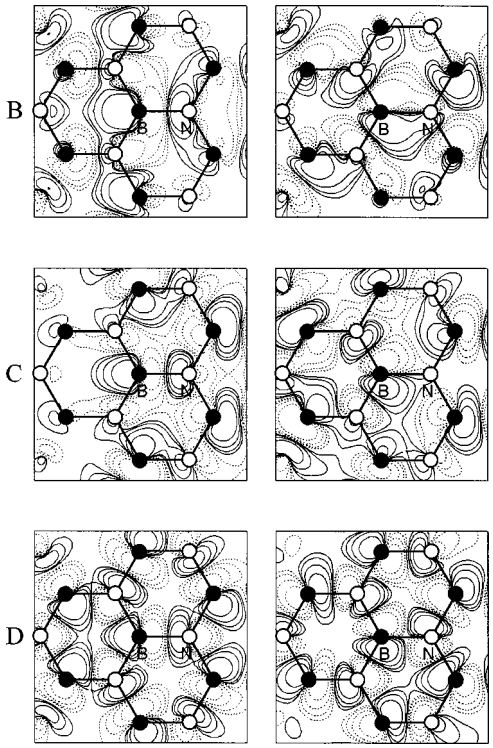

FIG. 6. Contour maps of pairs of the doubly degenerated wave functions responsible for peaks B, C, and D shown in Fig. 5 obtained for the $(B_7N_{12})^{15-}$ cluster at the transition state. Curves are drawn for ± 0.01, ± 0.02, ± 0.04, and ± 0.08, respectively. Solid and dotted curves are for positive values and negative values, respectively.

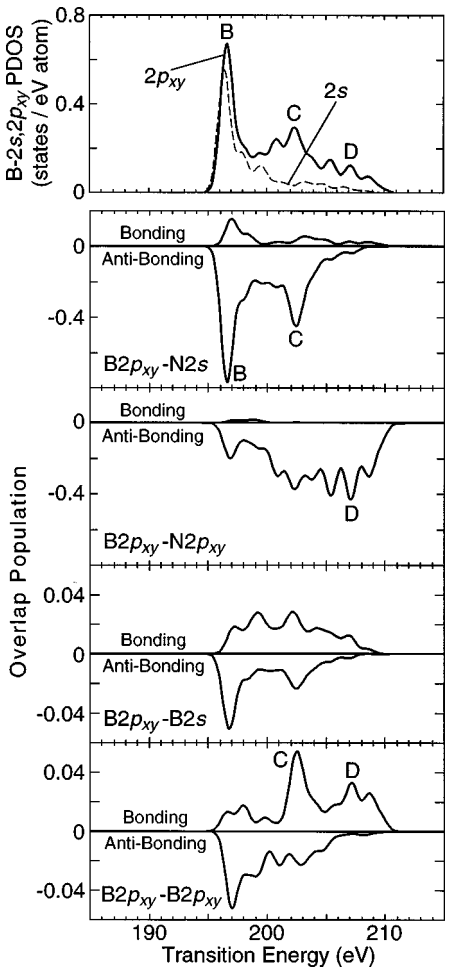

FIG. 7. Local B2s and p_{xy} PDOS by the $(B_{91}N_{108})^{51-}$ cluster at the transition state and the overlap population diagrams.

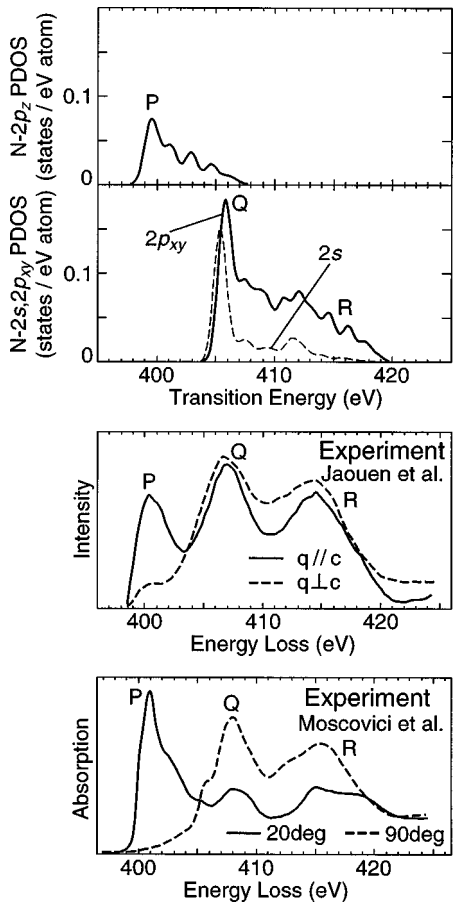

FIG. 9. Local (1st row) N-2p_z and (2nd row) N-2p_{xy} PDOS at the center of a model cluster h-$(B_{91}N_{108})^{51-}$ the transition state, in comparison with (3rd row) experimental N-K-edge ELNES by Jaouen *et al.* (Ref. 27) and (4th row) NEXAFS by Moscovici *et al.* (Ref. 21).

These features can be generated only when basis sets are extended to include B-3s and 3p. A sum of B-2p and B-3p PDOS using the $(B_7N_{12})^{15-}$ cluster at the Slater's transition state including B-3s and 3p orbitals as basis functions in extra is shown in Fig. 8. Peaks A and B are not changed by the extension. On the other hand, new peaks appear above peak C. Using the extended basis sets, peak D is made by the B-3p rather than the B-2p. With the increase of the transition energy, peak width increases in general. Further addition of extended basis functions may improve the reproduction of the high-energy features. However, this is out of the scope of the present paper, since the broader the peak becomes, the less information regarding its chemical environment it provides.

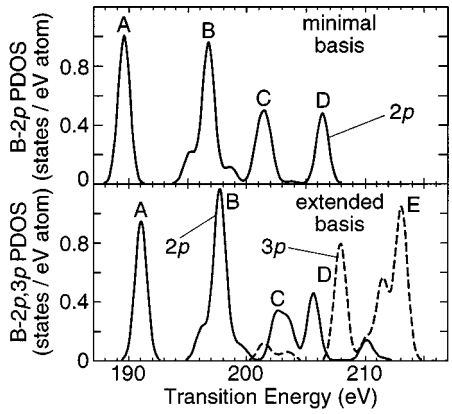

FIG. 8. The B-2/3p PDOS by the $(B_7N_{12})^{15-}$ cluster at the transition state (top) using minimal-basis sets (bottom) including B-3s and 3p orbitals as basis functions in extra.

Figure 9 shows experimental N-K-edge ELNES[27] and NEXAFS[21] from h-BN in comparison with theoretical N-2p_z and N-2p_{xy} PDOS by a N-centered cluster, $(N_{91}B_{108})^{51+}$. Similar to the case of the B-K edge, the inclusion of a half-filled core hole makes the first and second peaks pronounced. Agreement between experimental and theoretical spectra are satisfactory. Moscovici *et al.*[21] pointed out that the first peak of the N-K-edge NEXAFS (peak P) is much more broader than that of the B-K edge (peak A). They ascribed the fact to be due to the larger radius of N-2p_z orbital as compared with that of B-2p_z, leading to a larger overlap of the orbitals, which results in larger dispersion of the band. The bandwidth of the B-2p_z can be defined as the difference in peaks A and A′, since they have two extreme wave vectors as shown in Fig. 4. The A-A′ difference is as large as the width of the first peak of the N-K-edge spectrum. Therefore, the claim by Moscovici *et al.*[21] is found not to be the case.

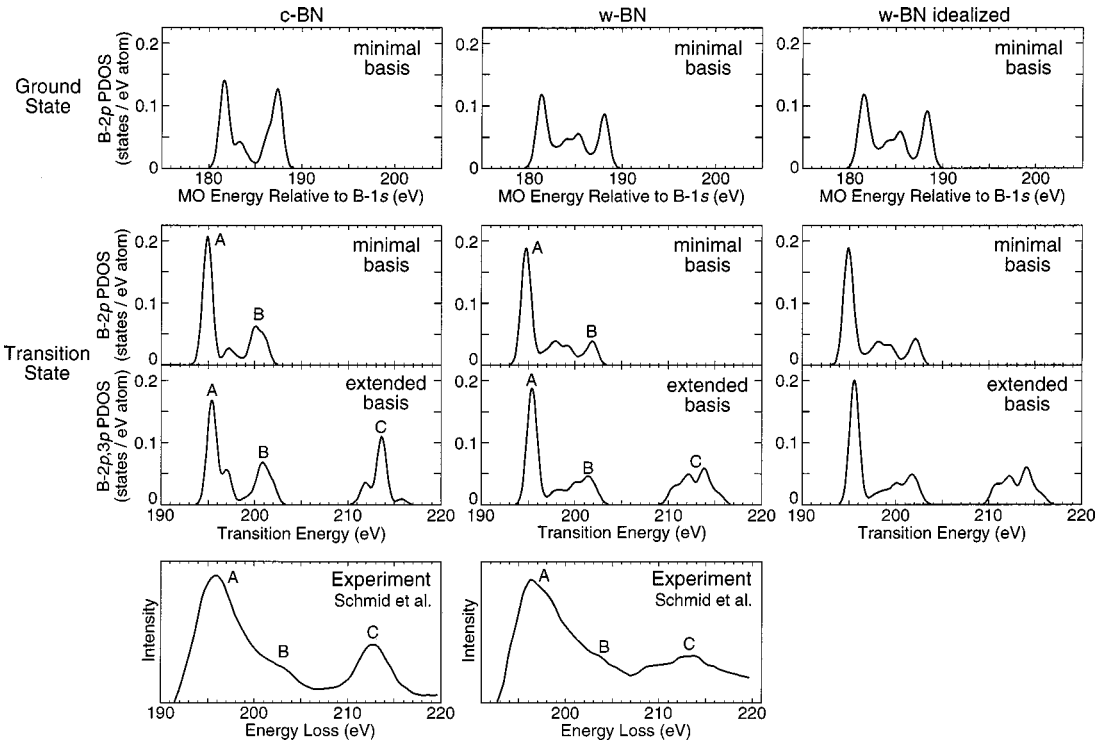

FIG. 10. Local B-2p PDOS for model clusters of (left column) c-BN, (middle column) w-BN, and (right column) w-BN, with idealized tetrahedrons. Clusters are c-$(B_{13}N_{28})^{45-}$ and w-$(B_{13}N_{29})^{48-}$. (1st row) results at the ground states, (2nd row) at the transition states with minimal basis-sets, and (3rd row) with the extended basis sets. Experimental B-K-edge ELNES by Schmid (Ref. 24) are compared.

Regarding absolute transition energies, theoretical results by Slater's transition-state method allowing temporary spin polarization (as denoted by transition energy in the figures) agree with experimental values within an error of 1% at both B-K and N-K edges. The transition energy is found to be almost independent of the cluster size.

IV. CUBIC AND WURTZITE BORON NITRIDES (c-BN,w-BN)

Cubic and wurtzite BN are both 4:4 coordinated, but their atomic arrangements are different at the second nearest-neighbor shells. B-K-edge ELNES from these two polytypes reported by Schmid[24] are shown in Fig. 10. Roughly speaking, B-N bonds in both c- and w-BN are all σ^* type and they are saturated. The intense peaks located at 196 eV has been ascribed to the σ^* interaction. Other than the intense peak (peak A), two peaks can be seen in the energy region below 220 eV. Both peaks B and C in the experimental spectra are seemingly broader in w-BN than in c-BN. Schmid[24] pointed out that a small difference at the low-energy shoulder of peak C is a fingerprint for the w-BN. However, he did not refer to the origin at all.

Figure 10 shows B-p PDOS by two clusters taken from c-BN and w-BN, i.e., c-$(B_{13}N_{28})^{45-}$ and w-$(B_{13}N_{29})^{48-}$, in comparison with experimental spectra. Calculations were made both at the ground and Slater's transition states. Minimal and extended basis sets were employed. The B-2p PDOS at the ground state in two systems well agree with those by the band-structure calculation using the orthogonal linear combination of atomic orbitals (OLCAO) method.[20] However, the intensity ratio of A to B, i.e., I_A/I_B, of the experimental spectra is not well reproduced by these ground-state calculations. When a core hole is included, I_A/I_B is remarkably increased in both c- and w-BN. This can be ascribed to the localization of the wave function responsible for peak A due to the presence of the core hole. The I_A/I_B in the experimental spectra are then reproduced. In other words, the presence of the core hole significantly alters the I_A/I_B in these two crystals.

Peak B is found to be sharper in c-BN as compared with w-BN, which agrees with the experimental spectra. Besides the difference in the stacking of the $[BN_4]$ tetrahedrons, they are slightly elongated in w-BN but are regular tetrahedrons in c-BN. In order to find the effect of the difference in the shape of tetrahedrons, an extra calculation for w-BN using perfect tetrahedrons was made as shown on the right panels of Fig. 10. As can be seen, the structure of B-2p PDOS is not sensibly changed by the idealization of the $[BN_4]$ tetrahedrons in w-BN. The difference between the width of peak B between c- and w-BN can, therefore, be ascribed to the difference in the manner of the tetrahedral stacking. The presence of a low-energy shoulder of peak C in the experimental spectrum as pointed out by Schmid,[24] although the shoulder peak does not clearly show up, may also be related to the broadening.

Peak C can only be reproduced when B-3s and 3p orbitals are included as basis functions in extra, which is the same as peak E in h-BN as found in Fig. 8. It can, therefore, be ascribed to the B-3p components. Similar to the case of peak B, peak C is broader in w-BN as compared with c-BN. The broadening is also seen in the wurzite structure with idealized $[BN_4]$ tetrahedrons. Thus, this can also be ascribed to the difference in the manner of tetrahedral stacking.

The absolute transition energies by theoretical calcula-

tions are in good agreement with experiments similar to the case of *h*-BN.

V. SUMMARY

First-principles molecular-orbital calculations of BN-polytypes, *h*-BN, *c*-BN, and *w*-BN, are conducted using model clusters. Effects of a core hole in the unoccupied density of states are systematically studied in order to reproduce and interpret experimental ELNES/NEXAFS at both B- and N-K edges. Major results can be summarized as follows: (1) Wave functions are found to localize significantly near the core hole, thereby changing their energies as well as their spatial distribution. They are very different from the Bloch states assumed in a band-structure calculation on the basis of structural unit cell. When the presence of the core hole is ignored, in other words at the ground state, small clusters such as *h*-(B_7N_{12}) exhibit better agreement with the experiment as compared with large clusters such as *h*-($B_{91}N_{108}$) because wave functions are made to localize in the small clusters. (2) Peak E in the B-K-edge spectrum of *h*-BN and peak C in the B-K-edge spectrum of *c*- and *w*-BN are not reproduced by the calculations using minimal basis functions. They emerge only when the basis set is expanded to include B-3*s* and 3*p*. (3) All of the other peaks in the B-K-edge spectrum of *h*-BN are interpreted in terms of chemical bondings among atomic orbitals using overlap population diagrams. Although peaks B, C, and D are all originated from B-$2p_{xy}$ orbitals, they are different in the magnitude of contributions of B-2*s* and N-2*s* as well as the number of nodes in the molecular orbital. (4) The N-K-edge spectrum of *h*-BN is well reproduced. Its first peak P is confirmed to be broader than the first peak A in the B-K-edge spectrum. (5) The B-K-edge spectra of *c*- and *w*-BN including their small differences are well reproduced. The difference in the experimental spectra are attributed not to the shape of the [BN_4] tetrahedrons but to the difference in the manner of tetrahedral stacking. (6) Regarding absolute transition energies, theoretical results by Slater's transition-state method allowing temporary spin polarization (as denoted by transition energy in the figures) agree with experimental values within an error of 1% at both B-K and N-K edges. The transition energy is found to be almost independent of the cluster size.

ACKNOWLEDGMENT

This work was supported by a Grant-in-Aid for General Scientific Research from the Ministry of Education, Sports, Science, and Culture of Japan.

[1] N. D. Browning, M. F. Chisholm, and S. J. Pennycook, Nature (London) **366**, 143 (1993); L. M. Brown, *ibid.* **366**, 721 (1993); D. M. Müller, Y. Tzou, R. Raj, and J. Silcox, *ibid.* **366**, 725 (1993); P. E. Batson, *ibid.* **366**, 727 (1993).

[2] R. Kuzuo, M. Terauchi, M. Tanaka, Y. Saito, and Y. Achiba, Phys. Rev. B **51**, 11 018 (1996).

[3] O. Stéphan, P. M. Ajayan, C. Colliex, F. Cyrot-Lackmann, and É. Sandré, Phys. Rev. B **53**, 13 824 (1996).

[4] D. Golberg, Y. Bando, M. Eremets, K. Kurashima, T. Tamiya, K. Takemura, and H. Yusa, J. Electron Microsc. **46**, 281 (1997).

[5] M. Terauchi, M. Tanaka, T. Matsumoto, and Y. Sato, J. Electron Microsc. **47**, 319 (1998).

[6] P. R. Wallace, Phys. Rev. **71**, 662 (1947).

[7] F. C. Chalkin, Proc. R. Soc. London, Ser. A **194**, 42 (1948).

[8] G. S. Painter and D. E. Ellis, Phys. Rev. B **1**, 4747 (1970).

[9] R. F. Willis, B. Fitton, and G. S. Painter, Phys. Rev. B **9**, 1926 (1974).

[10] N. A. W. Holzwarth, S. G. Luuie, and S. Rabii, Phys. Rev. B **26**, 5382 (1982).

[11] X. Weng, P. Rez, and H. Ma, Phys. Rev. B **40**, 4175 (1989).

[12] D. A. Fischer, R. M. Wentzcovitch, R. G. Carr, A. Continenza, and A. J. Freeman, Phys. Rev. B **44**, 1427 (1991).

[13] D. Denley, P. Perfetti, R. S. Williams, D. A. Shirley, and J. Stöhr, Phys. Rev. B **21**, 2267 (1980).

[14] R. A. Rosenberg, P. J. Love, and V. Rehn, Phys. Rev. B **33**, 4034 (1986).

[15] T. Fujikawa, J. Phys. Soc. Jpn. **52**, 4001 (1983).

[16] E. J. Mele and J. J. Ritsko, Phys. Rev. Lett. **43**, 68 (1979).

[17] R. Ahuja, P. A. Brühwiler, J. M. Willis, B. Johansson, N. Martensson, and O. Eriksson, Phys. Rev. B **54**, 14 396 (1996).

[18] I. Tanaka and H. Adachi, Phys. Rev. B **54**, 4604 (1996).

[19] J. C. Slater, *Quantum Theory of Molecules and Solids* (McGraw-Hill, New York, 1974).

[20] Y.-N. Xu and W. Y. Ching, Phys. Rev. B **44**, 7787 (1991).

[21] J. Moscovici, G. Loupias, Ph. Parent, and G. Tourillon, J. Phys. Chem. Solids **57**, 1159 (1996).

[22] H. Adachi, M. Tsukada, and C. Satoko, J. Phys. Soc. Jpn. **45**, 875 (1978).

[23] D. E. Ellis, H. Adachi, and F. W. Averill, Surf. Sci. **58**, 497 (1976).

[24] H. K. Schmid, Microsc. Microanal. Microstruct. **6**, 99 (1995).

[25] N. Watanabe, H. Hayashi, Y. Udagawa, K. Takeshita, and H. Kawata, Appl. Phys. Lett. **69**, 1370 (1996).

[26] The FLAPW calculation was done by ourselves using a program code WIEN97. [P. Blaha, K. Schwarz, and J. Luitz, Vienna University of Technology, 1997. This is the improved and updated version of the original copyrighted WIEN code, which was published by P. Blaha, K. Schwarz, P. Sorantin, and S. B. Trickey, Comput. Phys. Commun. **59**, 399 (1990)].

[27] M. Jaouen, G. Hug, V. Gonnet, G. Demazeau, and G. Tourillon, Microsc. Microanal. Microstruct. **6**, 127 (1995).